UNIVERSITY OF BIRMINGHAM
University of Birmingham Research at Birmingham

Vapour transport deposition of fluorographene oxide films and electro-optical device applications

Sharma, Rahul; Biroju, Ravi K.; Sinai, Ofer; Cohen, Hagai; Sahoo, Krishna Rani; Artel, Vlada; Alon, Hadas; Levi, Adi; Subrahmanyam, A.; Theis, Wolfgang; Naveh, Doron; Narayanan, Tharangattu N.

DOI:
10.1016/j.apmt.2018.08.015

License:
Creative Commons: Attribution-NonCommercial-NoDerivs (CC BY-NC-ND)

Document Version
Peer reviewed version

Citation for published version (Harvard):
Sharma, R, Biroju, RK, Sinai, O, Cohen, H, Sahoo, KR, Artel, V, Alon, H, Levi, A, Subrahmanyam, A, Theis, W, Naveh, D & Narayanan, TN 2018, 'Vapour transport deposition of fluorographene oxide films and electro-optical device applications', *Applied Materials Today*. https://doi.org/10.1016/j.apmt.2018.08.015

Link to publication on Research at Birmingham portal

Publisher Rights Statement:
Checked for eligibility: 07/12/2018

General rights
Unless a licence is specified above, all rights (including copyright and moral rights) in this document are retained by the authors and/or the copyright holders. The express permission of the copyright holder must be obtained for any use of this material other than for purposes permitted by law.

• Users may freely distribute the URL that is used to identify this publication.
• Users may download and/or print one copy of the publication from the University of Birmingham research portal for the purpose of private study or non-commercial research.
• User may use extracts from the document in line with the concept of 'fair dealing' under the Copyright, Designs and Patents Act 1988 (?)
• Users may not further distribute the material nor use it for the purposes of commercial gain.

Where a licence is displayed above, please note the terms and conditions of the licence govern your use of this document.

When citing, please reference the published version.

Take down policy
While the University of Birmingham exercises care and attention in making items available there are rare occasions when an item has been uploaded in error or has been deemed to be commercially or otherwise sensitive.

If you believe that this is the case for this document, please contact UBIRA@lists.bham.ac.uk providing details and we will remove access to the work immediately and investigate.

Download date: 28. Jun. 2022

Vapour Transport Deposition of Fluorographene Oxide Films and Electro-Optical Device Applications

Rahul Sharma[1#], Ravi K. Biroju[1#$], Ofer Sinai[2#@], Hagai Cohen[3], Krishna Rani Sahoo[1], Vlada Artel[2], Hadas Alon[2], Adi Levi[2], A. Subrahmanyam[4], Wolfgang Theis[5], Doron Naveh[2*], and Tharangattu N. Narayanan[1*]

[1]Tata Institute of Fundamental Research, Hyderabad-500107, India

[2]Faculty of Engineering, Bar-Ilan University, Ramat-Gan 5290002, Israel

[3]Department of Chemical Research Support, Weizmann Institute of Science, Rehovot 7610001, Israel

[4]Semiconductor Lab, Department of Physics, Indian Institute of Technology, Madras-600036, India

[5]Nanoscale Physics Research Laboratory, School of Physics and Astronomy, University of Birmingham, Birmingham- B15 2TT, United Kingdom

[$] (Present address) Nanoscale Physics Research Laboratory, School of Physics and Astronomy, University of Birmingham, Birmingham- B15 2TT, United Kingdom

[@] (Present address) The Israel Center for Advanced Photonics, Soreq NRC, Yavne 8180000, Israel

(*Corresponding Authors)(# Equally Contributing Authors)

*tnn@tifrh.res.in or tn_narayanan@ yahoo.com (T. N. N.), doron.naveh@biu.ac.il (D. N.)

Abstract

Fluorographene is one of the most interesting 2D materials owing to its span of electronic properties, from a conductor to wide-gap insulator, controlled by the compositional carbon to fluorine ratio. Unlike the chemically inert graphene, Fluorographene is recognized for its rich chemistry, particularly at ambient, allowing tailoring its physical properties. Here, we report onsingle step, catalyst free, wafer-scale synthesis of Fluorographene oxide (FGO) ultra-thinfilms (~ 4 nm thickness)by physical vapour deposition. The FGO, possessing 7% fluorine content, comprises few-nanometer domains of sp^2-sp^3 (fluorinated) carbon with high thermal stability, as confirmed by several analytical methods. We show that FGO can be utilized as an active hetero-layer ona few-layer MoS_2 field effect transistor (FET), significantly improving on the performance of MoS_2optoelectronic deviceswith an extended spectral response towards the near infrared and responsivity of up to 6A/W.The FGO-MoS_2band alignment as derived from the measured work function of FGO (4.7 eV) indicates a photoconductive gain mechanism with a fast transit time of holes mediated by FGO quasi-continuous defect states.

Keywords: Fluorographene Oxide, Wafer Scale Synthesis, Physical Vapour Deposition, Photodetector, Electronic Transport, Field Effect Transistor.

Graphical Abstract

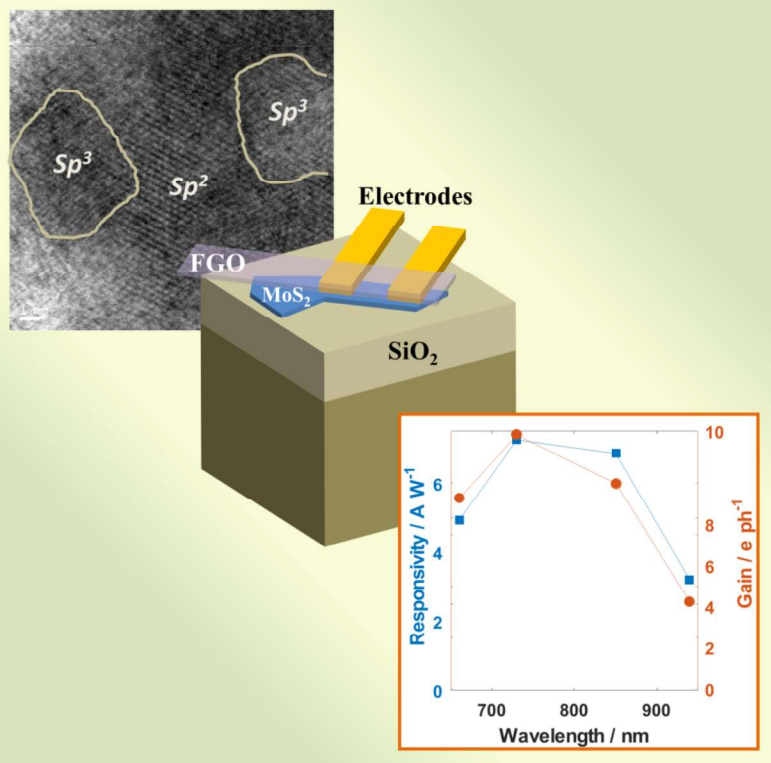

Development of a catalyst free, single step method for large area fluorographene oxide deposition and its applications in novel opt-electronic devices.

1.Introduction

Halogenated graphene derivatives have been found to possess remarkable physico-chemical properties[1], and covalently-bonded fluorographene (FG) derivatives are unique in this category[2]. The properties of FG can be tuned by varying the C/F ratio[3-5], and in particular its bandgap can be tuned from metallic (graphene, 0 eV) to insulating (3.8 eV) [6]. Ten layers of insulating FG were recently used as a gate dielectric in a graphene based field-effect transistor, displaying a record-high breakdown electric field and remarkable carrier mobility in the graphene channel [7]. The ability to control the bandgap of FG *via* fluorine content and its resulting electric properties make FG highly suitableforhetero-2D electronics [7], sensors, [4,8] and phototransistors [7, 9]. However, the synthesis of FG often relies on multi-step procedures based on the fluorination of graphene using fluorine-containing gases or precursors [10-11].These methods are based on catalytic growth of graphene upon which the fluorination process is subsequently applied, and consequently require transfer of the synthesized FG to a substrate of choice. Often, this multi-step synthesis procedure leaves residual impurities that can significantly impact the performance of electronic devices [7, 12]. While methods for the large-scale deposition of chemically derived FGs have been reported [2, 12], the synthesis of uniform FG over a large scale for electronic applications is still challenging with the existing multi-step methods [13-14]. Specifically, exfoliated FG is not considered a suitable candidate due to the high degree of disorder, defects and thickness variations, leading to non-uniformity in the electronic properties [7]. Thus, despite the superior properties, versatility, and suitability for various thin-device applications, a scalable method for achieving FG on an arbitrary substrate is still lacking. Fluorographene oxide(FGO) is a FG derivative containing sp^3 carbons with various oxygen species. FGO is also sought after for multiple applications[3]. In previous reports on FGO, the material is synthesized by chemical exfoliation of fluorinated graphite polymer using double step oxidation methods, and further development of thin films using FGO suspensions have always resulted in rough surfaces and limited thickness uniformity [3].

In this work, we demonstrate the preparation and characterization of large area highly crystalline FG/FGO films on various substrates, including Si/SiO_2, copper, glass, quartz and aluminium foil, by a catalyst free physical vapour transport deposition technique (PVD)using fluorographite polymer as a precursor. The deposited films' morphology, elemental composition, thickness and number of layers are investigated using micro-Raman spectroscopy, high-angle annular dark-field scanning transmission electron microscope (HAADF-STEM) imaging and X-ray photoelectron spectroscopy (XPS). The latter confirms the 2-dimensional nature of the films, which are ~4nm thick, corresponding to 6-7 layers. Because these analyses indicate the presence of both C-F and C-O functionalities, we henceforth term the deposited films FGO, as discussed in more detail below. The films are patterned using soft-lithography masks (pre-patterned poly dimethyl siloxane) with the aid of reactive oxygen plasma etching (Ar/O_2 (3:1)) and also with patterned resist using electron beam lithography (Figure 1).Finally, the outstanding potential for optoelectronic applications of PVD-grown FGO devices is demonstrated here. We fabricated FGO-MoS_2 FET hetero devices which demonstrate high responsivity in visible and near infrared (NIR) – up to 10-fold higher than silicon-based photodetectors. The advantages of our synthetic approach are its catalyst free growth on any substrate which is able to withstand the temperature of ~ 500-550 ^oC, it's easy scalability to large area deposition, and its simplicity as a single step growth method. Furthermore, both *x* and *n* of the fluorographite polymer ($(CF_x)_n$) precursor can ideally be controlled, leading to slight variations in the C/F ratios of the FGO films grown (not shown here).

2.Experimental

2.1Synthesis and transfer of Fluorographene Oxide (FGO) Films

2.1.1.Physical Vapor Deposition of FGO Films

Large area fluorographene oxide (FGO) films were fabricated using a physical vapor deposition (PVD) technique. The complete experimental procedure and source materials used for the FGO

deposition are detailed in the supporting information (figure S1(a-b)). Bulk Fluorinated graphite polymer powder (Sigma Aldrich; Cat. No. 42537; average particle size < 20 μm, ~60% fluorination$C_1F_{0.6}$) was used as the starting precursor for making FGO films. The source material and various substrates were placed in quartz boats, which were positioned in a tubular quartz chamber with the substrate ~ 8 cm downstream of the source material. The source end of the quartz tube was connected to the mass flow system and the substrate end was connected to the vacuum pump (see the Fig. S1(a)). The entire PVD system was inserted into a split tube muffle furnace. Argon/H_2 (10% H_2) was used as a carrier gas (200 standard cubic centimeters per minute, sccm) to transport the CF vapors onto the desired substrates. The partial hydrogen environment prevents oxidation of graphitic carbon during the deposition. The furnace was ramped up to the deposition temperature at a rate of 20 ˚C/min and maintained there for 20 minutes, during which FGO vapor from the source was deposited on the substrate. The furnace was then slowly cooled to 470 ˚C over 30 minutes. This slow cooling facilitates settling of the deposited FGO films in a controlled in-plane fluorination structure. Finally, the furnace was cooled down to room temperature.

The optimal source and substrate temperatures for controlled FGO deposition were determined to be 500 ºC, based on TGA/DTG analysis as follows: TGA measurements were performed on the FG source in both nitrogen (N_2) and air in order to estimate the thermal stability and sublimation temperature of each chemical species of carbon and fluorine (C-F, C-C and C=C) – see supporting information (Fig. S1(c)). This revealed that the C-F species decomposes at ~ 540 ˚C, leading us to select 500 ˚C for both source and substrate temperatures. We used various metal and insulating substrates, including aluminium (Al), copper (Cu), transparent quartz and Si/SiO_2 (300 nm). The source-substrate distances were varied between 7 and 8 cm.

2.1.2.Wet transfer of FG Films

The well-established method for wet transfer of chemical vapor deposition (CVD) graphene from Cu foil onto various substrates has been shown to cause minimal damage to the atomic layer [32, 33]. This was used in this work to transfer FGO films grown on Cu foil onto SiO2/quartz/PDMS substrates or Cu TEM grids [32]. A thin layer of poly(methyl methacrylate) (PMMA) in toluene (45 mg ml^{-1}) was spin coated on the Cu/ FGO layer, and the PMMA coated Cu/FGO was dried at 150 °C for 15 min in a hot oven. The underlying Cu was etched using aqueous $Fe(NO_3)_3$ etchant solution. The FGO/PMMA floating on the etchant solution was rinsed with deionized water several times to remove residual PMMA and metal impurities. It was then scooped and transferred on to the desired substrate manually, and subsequently dried in the oven for 1 h at 180 °C. Finally, the samples were dipped in acetone several times to remove the PMMA from the FGO layers. A schematic description of the wet transfer of PVD grown FGO on Cu is shown in the supporting information figure S5.

Note that FGO grown on other semiconducting/insulating substrates (such as Si/SiO_2) can be directly used for patterning and device fabrication and need not be transferred.

2.2.Film Characterization

Raman spectroscopy measurements of as-grown FGO were performed with a high-resolution commercial spectrometer (Renishaw, Invia), with excitation wavelength 532 nm. HRTEM measurements were performed with a JEOL 2100 TEM at an operating voltage of 200 kV. Temperature dependent morphology and crystal structure of FGO films were studied using in-situ Raman spectrometry and electron microscopy. Temperature dependent (T = 50-800˚C) in-situ Raman studies were performed using an in-situ micro-Raman spectrometer, where the sample was placed in a Linkam cell. Temperature dependent (T = 100-400 ˚C) electron microscopy was performed using an in-situ heating holder, containing a high-resolution transmission electron microscope (HRTEM) and a dark/bright field scanning transmission electron microscope

(STEM). In particular, high resolution micrographs of sp^2 and sp^3 hybridized carbon domains were obtained using a 200 kV aberration-corrected STEM (JEM 2100F) in the high-angle annular dark-field (HAADF) mode.

X-ray photoelectron spectroscopy (XPS) measurements were carried out using a Kratos AXIS-Ultra DLD spectrometer with a monochromatic Al kα source at power of 75 W and detection pass energies in the 20-80 eV range. Measurements were performed at two emission angles, 0 and 65 □, with respect to the surface normal. Beam induced damage was tested by performing a number of repeated scans on given sample spots, yielding high sample stability. Testing of the electrical properties of the sample included application of the electron flood gun (eFG), with which efficient surface conductivity was confirmed.

Surface work function measurements with Kelvin probe were performed with a home built system [34]. The tip of the Kelvin probe head used was stainless steel of 1.0 mm in diameter; the surface work function of the tip is 4.625 eV (calibrated with pyrolytic graphite). The reported contact potential (CPD) values are with reference to the stainless steel; these CPD values are directly proportional to the changes in the surface work function of the sample under test.

$$qV_{cpd} = \Phi_{tip} - \Phi_{sample} \quad (1)$$

The bulk function, in general, will be different from the surface work function. The surface work function is the energy required to remove an electron from the surface Fermi level to the vacuum level. The work function of FGO is calculated as: 4.625 – (-0.074) = 4.699 eV.

2.3.Fabrication of MoS_2-FGO stacks

MoS_2 flakes (3-4 layer thick, as estimated from Raman measurements – shown in the SI– and optical microscope contrast) were mechanically exfoliated(from bulk undoped MoS_2 crystal, source: HQ Graphene, Netherlands) on 285 nm SiO_2 supported by p^+-Si that is used as the back

gate. Electrodes were patterned using electron-beam lithography, followed by a gentle plasma treatment (5 sec C_2F_6 plasma at low RF power) prior to metallization with 10/60 nm of Ti/Pd. The devices were then annealed for 2 hours at 200°C in vacuum (P = 10^{-6}Torr). FGO was transferred on top of the devices following the procedure described for graphene transfer using ethylene vinyl acetate (EVA) [35]. The FGO was patterned using AZ negative (NLOF 2020) resist and removed from unwanted areas using O_2 RF plasma.

2.4.Electrical and Electro-Optical Measurements

A wire-bonded chip mounted on a Montana Instruments Cryostation at which I-V transfer curves were measured using a Keysight B2912A Source/Measure Unit. Photocurrents were measured using a Stanford Research Systems SR830 lock-in amplifier, with a Femto DLPCA-200 low-noise current pre-amplifier. The light sources were Thorlabs LED monochromatic sources at 660, 730, 850 and 940 nm (M660L4, M730L4, M850L3, M940L3) providing uniform illumination of the entire chip. All electrical and electro-optical measurement sweeps were run in both forward and back directions. Since no noticeable hysteresis was found, for clarity only the forward scans are shown above.

3. Result and Discussion

Figure 1(a) displays an optical micrograph of as-grown FGO on a Si/SiO_2 substrate, where a mask was used in order to leave part of the SiO_2 substrate bare. The unmasked region shows an outstanding uniformity of the FGO film. Micro-Raman spectra of both regions are shown in figure 1(b).The D-band (1350 cm^{-1}), G-band (1590 cm^{-1}) and the broad line shape of the 2D-band (2700 cm^{-1}) are all visible in the unmasked (deposited) regions. Figure 1(c, d, e) represents the Raman mappings of a similar partially masked sample, showing the D-band intensity, the G-band intensity, and their ratio (I_D/I_G), respectively. The Raman mappings confirm the homogeneity of the FGO layer over the large area, and the larger value of I_D/I_G is significant for controlled in-plane fluorination over the sp^2-sp^3 carbon sites. The I_D/I_G ratio found indicates

an intermediate degree of fluorination, unlike carbon monofluoride $(-CF-)_n$ where no graphitic Raman signature is expected [15].FGO films grown on quartz feature good optical transparency (80% transmittance) in the visible region (figure S1d).The morphological features of as-grown FGO are estimated from high resolution field emission scanning electron microscopy (FESEM) image. Figure 1(f) shows contrast obtained at a partially masked region of an FGO film grown on a SiO_2 substrate. The inset shows a high resolution FESEM image of the unmasked region, consisting of nanometer sized regions of two different contrasts. These regions are further characterized using HRTEM and STEM and identified as nanometer-sized sp^2-sp^3 regions (see below).The large area patternability of these FGO films is demonstrated in figure 1(g), where a pre-patterned PDMS mask was applied to FGO on Si/SiO_2,followed by reactive oxygen plasma etching. Large area growth of FGO was achieved using this method: we deposited a uniform FGO layer on 15 cm X 15 cm aluminium foils, characterization details are shown in the supporting information figure S1 (the FGO-covered foils are shown in figure S1e and S1f; the associated alteration of the foil wettability is shown in figure S1f, and Raman spectra from widely spaced points on the sample (S1g) indicate uniformity of the FGO coverage).

Further investigation of the sp^2-sp^3 carbon domains and their grain sizes in the as-grown FGO was performed by high angle annular dark field scanning transmission electron microscopy (HAADF-STEM). Figures 2(a-b) show dark and bright field (respectively) STEM images of the FGO transferred onto the TEM Cu grid (see the experimental section and supporting information for details). Insets show the lattice pattern of the single FGO flake, corresponding to the hexagonal lattice of sp^2 carbon in the labelled domains. The variation in the HAADF intensity within flakes is attributed to the thickness uniformity of FGO films and its resulting electron scattering. Figure 2(c) depicts a high-resolution HAADF-STEM image of a single flake with the sp^2 and sp^3 carbon domains labelled, and the corresponding bright field STEM image is shown figure 2(d). The hexagonal lattice diffraction pattern of sp^2 carbon is clearly observed in the FFT

of the rectangular marked portion in figure 2(d) (left inset in figure 2(c)), while other marked portions correspond to sp^3 carbon sites within a single FG flake. HAADF-STEM imaging confirms the number of atomic layers in FGO films to be 6-7 layers (see supporting information, figure S3). This thickness estimate is also supported by the XPS results below.

As an examination of the chemical stability of PVD-deposited FGO, as-grown films were immersed in several different solvents including acetone, THF (tetrahydrofuran), and toluene for a period of several weeks. After immersion, the fluorine content of the films was examined and found to show only a minor decrease. FGO may contain covalent, semi ionic and ionic bonds between carbon and fluorine due to the high electronegativity of fluorine. Polar solvents have been reported to attack ionic and semi ionic C-F bonds [3]. Thus, the stability of the fluorine content after extensive immersion in polar solvents indicates that most of the C-F bonds in the deposited films are covalent in nature.

The large area electronic uniformity of the deposited films is confirmed by surface work function analysis using Kelvin probe microscopy. Figure 3(a) shows the contact potential difference (CPD) of FGO films deposited on Si/SiO_2over a 1 mm x 0.5 mm surface. The work function of FGO is found to be4.699 eV. By analogy with a previously reported system involving fluorinated multi-layer graphene, this value points to a fluorine content of 7% [16].The small variation of CPD values over a mm^2 area is an indication of the excellent uniformity of the electronic properties of the deposited FGO material.

XPS analysis of as-grown and vacuum annealed (400 °C for 1 hour) samples on a SiO_2substrate was performed at two different emission angles, providing quantitative information that supports the expected structure of a thin FGO layer on SiO_2. Representative spectra are shown in figure4. The C 1s peak exhibits a broad tail towards high binding energies. Such a tail is typical to graphene, in which shake-up processes gain significant intensity [17]. However, in the present case the tail is rather distorted and additional signals are superimposed on it, with energies

corresponding to the chemically shifted C-F signal and, possibly, C-Ox species. The origin of this extended tail is discussed further in the supporting information.

Quantitatively, it is found that C/F ratios are around 15 (see table 1) for both as-grown and annealed samples, *i.e.*, ~7% fluorination, in excellent agreement with the Kelvin probe results above. The thickness of the graphene-like layer is estimated to be around 3-4 nm. After annealing, a small change only is encountered in both the C/F ratio and the estimated thickness, which indicates a remarkably high thermal stability of the fluorination. This thermal stability is also confirmed by thermo gravimetric analysis and temperature-dependent TEM (see supporting information). The observed differences are attributed to desorption (during annealing) of residual organic contaminants that reside on top of the graphene, as well as to loss of some top F atoms. The latter conclusion is supported by the observed increase in the C/F ratio at grazing (65°) emission (exceeding the calculated attenuation corrections – not shown), indicating that, on average, F atoms in the annealed case reside at sites deeper than C atoms. Thus, F atoms buried in between graphene sheets and at the interface with the silica are protected against loss upon annealing.

It should be noted that a thin, sub-nm, layer of suboxide is formed at the interface between the FGO and the SiO_2 (silica). This observation is based on the emergence of two chemically different O and Si components, as shown in the supporting information and depicted in Table 1. While the oxidation states and stoichiometry of the substrate silica appear consistent, a naïve interpretation of the suboxide signals points to inconsistent stoichiometry. We attribute the latter to O diffusion into the graphene and the (partial) oxidation of the deposited layer. The estimated amount of diffused-O is roughly half the amount of F. The presence of C-O species is also consistent with the relatively high tail of the C 1s line described above.

Table 1: XPS-derived atomic concentrations (%) and related values. Two silica components are resolved in each of the O and Si signals, denoted Ox1 for the stoichiometric silica and Ox2 for the layer of suboxide

that is formed at the interface with the FGO. Corrections for photoelectron attenuation lead to a reasonable 1:2 stoichiometry in Ox1, however the Ox2 stoichiometry reveals an extra amount of O (roughly half of the F amount). The thickness estimations (d_{FG} and d_{subox}) do not account for oxygen diffusion between the oxide and the deposited layer.

	Emission angle	**F**	**C**	**O1**	**O2**	**Si1**	**Si2**	**C/F**	**d_{FG} (nm)**	**d_{subox} (nm)**
As-grown	**0**	4.41	66.38	13.38	4.63	8.60	2.51	15.06	4.0	0.8
	65 □	4.54	74.82	5.14	6.77	3.3	5.44	16.48	3.0	1.3
Annealed	**0**	4.21	57.96	18.41	4.12	12.32	2.71	13.8	3.2	0.4
	65 □	4.04	70.25	~6.36	~7.37	6.35	5.3	17.4	1.9	0.6

Independent structural information can be obtained from the analysis of the XPS line shifts caused under application of the neutralizer; an electron flood gun (eFG), operated at 1.9A and 4.3 V [18], as summarized in Table 2. Notably, the silica lines (O and Si) undergo slightly higher shifts than those of the C 1s. This indicates that charges are evacuated to ground mainly via surface conduction (laterally), as opposed to vertical mechanisms exploiting the doped wafer underneath. Besides the confirmation obtained from the latter as of the vertical ordering of layers [18], which is indeed fully consistent with all other techniques, we get here independent evidence for relatively high conductivity of the FGO film, a feature further discussed below. Note that after annealing we get larger shifts, which reflects a decrease in the surface states available for transport and, in this respect, improved system integrity.

Table 2: Line shifts (in meV) detected under fixed eFG conditions. Unless otherwise specified, the experimental error is ±10 meV.

sample	C	F	O	Si
As-grown	140	130±20	165	150
Annealed	265	300	300	290

To examine the electrical and optoelectronic behaviour of devices based on PVD-deposited FGO, we fabricated and characterized several FGO/MoS_2 heterostructure devices. Figure 5a describes the device structure schematically (see experimental section for full details of the fabrication process). Few-layer exfoliated MoS_2FET devices were fabricated on the surface of 285 nm thick SiO_2on *p*+- Si that performed as the back gate (BG). As-grown FGO films were then transferred onto the MoS_2channels and contacted separately. Figure 5b shows an optical micrograph of several devices, with a red arrow indicating the device from which the representative data shown here is taken.

The electrical characteristics of the devices were examined (Figure 5c)showing the drain current resolved by back gate voltage (V_{BG}), at temperatures of 300K and 120K. The positive threshold voltage matches the expected *n*-FET behaviour for MoS_2 [19, 20]. However, at room temperature, a leakage current of ~5nA is observed, which we attribute to the conductivity of FGO. Thus, below(above)a threshold voltage (~30 V) the conduction is dominated by FGO(MoS_2),respectively. This leakage current is significantly suppressed at low temperature. It was confirmed to be carried by FGO by measuring a bare FGO device at varying temperatures (figure S4), resolving the temperature-dependent leakage currents of FGO.

The photoresponse of the devices was measured at a temperature of 120K at several wavelengths (λ)and back-gate voltages, as shown in figure 5. Figure 5d shows the photocurrent *versus* illumination power at grounded back-gate ($V_{BG} = 0$) at wavelengths of 850 nm and 940 nm, at the absorption edge of few-layer and bulk MoS_2, respectively. The responsivity of the device (slope of curves) is largest at the lowest illumination powers and is strongly dependent on

the gate bias (Figure 5e). Interestingly, the response of the device is higher at negative gate bias and gradually decays at positive voltage, towards complete quenching above the threshold voltage of 30 V. This trend is opposite to gate resolved photocurrents of pureMoS_2 [20, 21].Finally, the wavelength dependence of the maximum responsivity(at V_{BG} = -10 V) and corresponding photoconductive gain are shown in figure 5f, in which gain as high as 10 is demonstrated for λ = 730 nm.

The gate resolved photocurrent and spectral response of the devices qualitatively differ than those of bare MoS_2, indicating that photocurrents are dominated by the FGO-MoS_2 heterostructure rather than by the MoS_2 alone (see also supporting information). The work function measured for the FGO (4.7 eV, see above) aligns ~0.4 eV below the MoS_2 conduction band (CB) [22, 23]. The observed disorder and clusters of sp^2-sp^3 domains in FGO (see figure 2) are assumed to result in a quasi-continuous band of defect states in the FGO film. Thus, both the trapping of photo-excited electrons at defects and a faster transit time of holes/electrons can be mediated by FGO. Below the threshold voltage, defect states overlap the valence band (VB) and Fermi level, resulting in dark currents (figure 5c) and (under illumination) a short transit time of holes, contributing to the observed photoconductive gain [24, 25]. Above the threshold voltage, Pauli blocking and fast recombination lead to quenching of the photoresponse. Figure 6 illustrates the photoconductive mechanism schematically. Notably, MoS_2 devices reported in previous literature show very low responsivity above λ ~ 700 nm, if at all [20, 26-31] (see table S1). Furthermore, bare few-layer MoS_2 devices consistently show responsivities at an order of magnitude lower than our few-layer MoS_2/FGO devices, even at wavelengths shorter than ~700 nm [26-28]. By combining MoS_2 with PVD-grown FGO, we extend the spectral response of MoS_2 and achieve a significant photoconductive gain.

4. Conclusion

In conclusion, PVD based catalyst-free large-area deposition of high quality, thin (~4 nm) FGO films was demonstrated on a variety of substrates. The films were extensively characterized by micro-Raman, HAADF-STEM, XPS and Kelvin probe, all of which point to a degree of fluorination of roughly 7% (a 15-to-1 ratio of C to F), and possibly some fraction of oxygen species. The films are highly uniform at the microscopic level, with a mosaic structure comprising sp^2-and sp^3-hybridized domains revealed at the nanometer level by HAADF-STEM. The patterning of the FGO films using soft-mask or electron beam lithography demonstrates their easy processability, and allowed us to highlight the potential for optoelectronic applications of PVD-grown FGO films by combining them with MoS_2 FET devices. The optoelectronic performance of the heterostructure devices was found to be inseparably linked to the unique structure and properties of the FGO, leading to enhanced photocurrent generation and gain as high as 10 at visible and NIR light, thus improving on bare MoS_2-FET based photodetectors significantly, and even outperforming Si-based photodiodes with respect to their photoresponse. The versatility, easy scalability and simplicity of its growth procedure, coupled with its remarkable optoelectronic properties, make PVD-grown FGO an attractive candidate for integration in innovative future devices and other applications.

Acknowledgement

OS is grateful for the help of Ms. Michal Wasserman with the electrical measurements and microscopy of some of the samples. DN thanks the Israel Science Foundation for grant No. 1055/15. TNN acknowledges the funding support from Tata Institute of Fundamental Research (TIFR), India. TNN also acknowledges DST-SERB, India for the funding support in the form of extra-mural research grant for working on van der Waals solids based structures (EMR/2017/000513). RKB acknowledges Marie-Sklodowska-Curie individual fellowship under EU H2020 programme (H2020_IF_2017; Grant Number: 750929) and postdoctoral fellowship from SERB-NPDF (PDF/2016/002642), India. We thank Dr. Balakrishna Ananthoju and Prof.

Robert Dryfe, The University of Manchester for the Raman streamline mapping measurements of FG samples.

Electronics Supporting Information

Supporting Information is Provided

References:

[1] F. Karlický, K. Kumara Ramanatha Datta, M. Otyepka, R. Zbořil, Halogenated Graphenes: Rapidly Growing Family of Graphene Derivatives, ACS Nano 7(8) (2013) 6434-6464.
[2] R. Romero-Aburto, T.N. Narayanan, Y. Nagaoka, T. Hasumura, T.M. Mitcham, T. Fukuda, P.J. Cox, R.R. Bouchard, T. Maekawa, D.S. Kumar, S.V. Torti, S.A. Mani, P.M. Ajayan, Fluorinated Graphene Oxide; a New Multimodal Material for Biological Applications, Adv. Mater. (Weinheim, Ger.) 25(39) (2013) 5632-5637.
[3] K.K. Tadi, S.K. Bikkarolla, K. Bhorkar, S. Pal, N. Kunchur, I. N, S. Radhakrishnan, R.K. Biroju, T.N. Narayanan, Defluorination of Fluorographene Oxide via Solvent Interactions, Particle & Particle Systems Characterization (2017) 1600346-n/a.
[4] K.K. Tadi, S. Pal, T.N. Narayanan, Fluorographene based Ultrasensitive Ammonia Sensor, Scientific Reports 6 (2016) 25221.
[5] S. Boopathi, T.N. Narayanan, S. Senthil Kumar, Improved heterogeneous electron transfer kinetics of fluorinated graphene derivatives, Nanoscale 6(17) (2014) 10140-10146.
[6] K.-J. Jeon, Z. Lee, E. Pollak, L. Moreschini, A. Bostwick, C.-M. Park, R. Mendelsberg, V. Radmilovic, R. Kostecki, T.J. Richardson, E. Rotenberg, Fluorographene: A Wide Bandgap Semiconductor with Ultraviolet Luminescence, ACS Nano 5(2) (2011) 1042-1046.
[7] K.-I. Ho, C.-H. Huang, J.-H. Liao, W. Zhang, L.-J. Li, C.-S. Lai, C.-Y. Su, Fluorinated Graphene as High Performance Dielectric Materials and the Applications for Graphene Nanoelectronics, Scientific Reports 4 (2014) 5893.
[8] V. Urbanova, F. Karlicky, A. Matej, F. Sembera, Z. Janousek, J.A. Perman, V. Ranc, K. Cepe, J. Michl, M. Otyepka, R. Zboril, Fluorinated graphenes as advanced biosensors - effect of fluorine coverage on electron transfer properties and adsorption of biomolecules, Nanoscale 8(24) (2016) 12134-12142.
[9] M. Zhong, D. Xu, X. Yu, K. Huang, X. Liu, Y. Qu, Y. Xu, D. Yang, Interface coupling in graphene/fluorographene heterostructure for high-performance graphene/silicon solar cells, Nano Energy 28(Supplement C) (2016) 12-18.
[10] Y. Yang, G. Lu, Y. Li, Z. Liu, X. Huang, One-Step Preparation of Fluorographene: A Highly Efficient, Low-Cost, and Large-Scale Approach of Exfoliating Fluorographite, ACS Appl. Mater. Interfaces 5(24) (2013) 13478-13483.
[11] P. Gong, Z. Wang, J. Wang, H. Wang, Z. Li, Z. Fan, Y. Xu, X. Han, S. Yang, One-pot sonochemical preparation of fluorographene and selective tuning of its fluorine coverage, J. Mater. Chem. 22(33) (2012) 16950-16956.

[12] T.N. Narayanan, R.K. Biroju, V. Renugopalakrishnan, Fluorographene: Synthesis and sensing applications, J. Mater. Res. (2017) 1-12.
[13] R. Padhye, A.J.A. Aquino, D. Tunega, M.L. Pantoya, Fluorination of an Alumina Surface: Modeling Aluminum–Fluorine Reaction Mechanisms, ACS Appl. Mater. Interfaces 9(28) (2017) 24290-24297.
[14] R. Ye, X. Han, D.V. Kosynkin, Y. Li, C. Zhang, B. Jiang, A.A. Martí, J.M. Tour, Laser-Induced Conversion of Teflon into Fluorinated Nanodiamonds or Fluorinated Graphene, ACS Nano (2018).
[15] R.R. Nair, W. Ren, R. Jalil, I. Riaz, V.G. Kravets, L. Britnell, P. Blake, F. Schedin, A.S. Mayorov, S. Yuan, M.I. Katsnelson, H.-M. Cheng, W. Strupinski, L.G. Bulusheva, A.V. Okotrub, I.V. Grigorieva, A.N. Grigorenko, K.S. Novoselov, A.K. Geim, Fluorographene: A Two-Dimensional Counterpart of Teflon, Small 6(24) (2010) 2877-2884.
[16] S.D. Sherpa, J. Kunc, Y. Hu, G. Levitin, W.A.d. Heer, C. Berger, D.W. Hess, Local work function measurements of plasma-fluorinated epitaxial graphene, Appl. Phys. Lett. 104(8) (2014) 081607.
[17] T. A., Practical surface analysis, 2nd edn., vol I, auger and X-ray photoelectron spectroscopy. Edited by D. Briggs & M. P. Seah, John Wiley, New York, 1990, 657 pp., price: £86.50. ISBN 0471 92081 9, J. Chem. Technol. Biotechnol. 53(2) (1992) 215-215.
[18] A.H. Ilanit Doron Mor, Alexander Vaskevich, Tamar van der Boom-Moav, Abraham Shanzer, Israel Rubinstein, Hagai Cohen, Controlled surface charging as a depth-profiling probe for mesoscopic layers, Nature 406 (2000) 382-385.
[19] O.V. Yazyev, A. Kis, MoS2 and semiconductors in the flatland, Materials Today (0).
[20] O. Lopez-Sanchez, D. Lembke, M. Kayci, A. Radenovic, A. Kis, Ultrasensitive photodetectors based on monolayer MoS2, Nat Nano 8(7) (2013) 497-501.
[21] H.L. Zongyou Yin, Hong Li, Lin Jiang, Yumeng Shi, Yinghui Sun, Gang Lu, Qing Zhang, Xiaodong Chen and Hua Zhang, Single-Layer MoS2 Phototransistors, ACS Nano 6(1) (2011) 74-80.
[22] H.-Y.C. Saptarshi Das, Ashish Verma Penumatcha and Joerg Appenzeller, High Performance Multilayer MoS2 Transistors with Scandium Contacts, Nano Letters 13(1) (2012) 100-105.
[23] J.L. Jong Hun Kim, Jae Hyeon Kim. Hwang, Changgu Lee and Jeong Young Park, Work function variation of MoS2 atomic layers grown with chemical vapor deposition: The effects of thickness and the adsorption of water/oxygen molecules, Applied Physics Letters 106 (2015).
[24] W.H. Hehai Fang, Photogating in Low Dimensional Photodetectors, Advanced Science 4(12) (2017) 2198-3844.
[25] G. Konstantatos, M. Badioli, L. Gaudreau, J. Osmond, M. Bernechea, F.P.G. de Arquer, F. Gatti, F.H.L. Koppens, Hybrid graphene-quantum dot phototransistors with ultrahigh gain, Nat Nano 7(6) (2012) 363-368.
[26] D. Kufer, G. Konstantatos, Highly Sensitive, Encapsulated MoS2 Photodetector with Gate Controllable Gain and Speed, Nano Lett. 15(11) (2015) 7307-7313.
[27] D.-S. Tsai, K.-K. Liu, D.-H. Lien, M.-L. Tsai, C.-F. Kang, C.-A. Lin, L.-J. Li, J.-H. He, Few-Layer MoS2 with High Broadband Photogain and Fast Optical Switching for Use in Harsh Environments, ACS Nano 7(5) (2013) 3905-3911.

[28] S. Lee, Y. Park, G. Yoo, J. Heo, Wavelength-selective enhancement of photo-responsivity in metal-gated multi-layer MoS2 phototransistors, Appl. Phys. Lett. 111(22) (2017) 223106.
[29] W. Tang, C. Liu, L. Wang, X. Chen, M. Luo, W. Guo, S.-W. Wang, W. Lu, MoS2 nanosheet photodetectors with ultrafast response, Appl. Phys. Lett. 111(15) (2017) 153502.
[30] C. Woong, C.M. Yeon, K. Aniruddha, L.J. Hak, C. Gi-Beom, H.S. Cheol, K. Sangsig, K. Jeongyong, J. Debdeep, J. Jinsoo, K. Sunkook, High-Detectivity Multilayer MoS2 Phototransistors with Spectral Response from Ultraviolet to Infrared, Adv. Mater. (Weinheim, Ger.) 24(43) (2012) 5832-5836.
[31] W. Jing-Yuan, C.Y. Tea, L. Shunpu, Z. Tong, W. Junzhan, S.P. Kumar, C. Daping, Broadband MoS2 Field-Effect Phototransistors: Ultrasensitive Visible-Light Photoresponse and Negative Infrared Photoresponse, Adv. Mater. (Weinheim, Ger.) 30(7) (2018) 1705880.
[32] R.K. Biroju, P.K. Giri, Defect Enhanced Efficient Physical Functionalization of Graphene with Gold Nanoparticles Probed by Resonance Raman Spectroscopy, J. Phys. Chem. C 118(25) (2014) 13833-13843.
[33] R.K. Biroju, P.K. Giri, S. Dhara, K. Imakita, M. Fujii, Graphene-Assisted Controlled Growth of Highly Aligned ZnO Nanorods and Nanoribbons: Growth Mechanism and Photoluminescence Properties, ACS Appl. Mater. Interfaces 6(1) (2013) 377-387.
[34] A.K. Subrahmanyam, S, The Kelvin Probe for Surface Engineering: Fundamentals and Design, CRC Press2010.
[35] J.-Y. Hong, Y.C. Shin, A. Zubair, Y. Mao, T. Palacios, M.S. Dresselhaus, S.H. Kim, J. Kong, A Rational Strategy for Graphene Transfer on Substrates with Rough Features, Adv. Mater. (Weinheim, Ger.) 28(12) (2016) 2382-2392.

Figures

Figure 1: (a) Optical Microscope (OM) image of as-grown FG film on a partially-masked SiO_2 substrate. The red and black circles denote masked and unmasked regions, respectively. (b) Corresponding Raman signatures of the FGO film with marking of D and G- bands.(c-e) Raman mappings of intensities of (c) D-band, (d) G- band and (e) I_D/I_G from a partially masked sample, as recorded with 532nm laser excitation. (f) FESEM image of the as-grown FGO scanned at masked and unmasked regions. Inset: high resolution FESEM image showing the closely packed few layered FG flakes. (g) FESEM image of an as-grown FGO film on SiO_2 substrate after patterning using a soft lithographic mask.

Figure 2: High Angle Annular Dark Field (HAADF) Scanning Transmission Electron microscopy (STEM) imaging of FGO film. (a) HAADF and (b) corresponding bright field STEM images of as-transferred closely packed few layer (6-7 layers) FGO flakes. Insets show the atomic lattice patterns of the single FGO flake. (c) HAADF and (d) bright-field STEM images showing the in-plane fluorine (F) functionalized FGO flake.sp^2 and sp^3 hybridised carbon lattice patterns are clearly visible within a single flake. The insets in (c) are the FFT (left) and IFFT (right) images of the marked rectangular portion of (d).

Figure 3: Contact potential difference (CPD) Kelvin Probe (KP) analysis of as-grown FG film

Figure 4: Representative XPS data at normal emission angle, taken from FGO grown on SiO_2before (solid blue lines) and after (dashed orange lines) vacuum annealing at 400 °C for 1 hour: (a) the C 1s and (b) the F 1s core lines. The dotted yellow curves in (b) present curve fitting components.

Figure 5: Electrical and electro-optical behaviour. (a) Schematic of a MoS_2-FG device structure. (b) Optical microscope image of several few-layer MoS_2 devices, taken prior to FG transfer for a better view of the underlying device structure. The white scale bar is 5 μm. Blue shaded flakes are MoS_2. After transfer, the FG outside of the dotted red line was removed by plasma etching. Results in panels (c)-(f) are from the channel indicated by the red arrow. (c) Drain current I_D as a function of back-gate voltage V_{BG}, at two different temperatures. In both cases V_D = 0.5 V. (d) Measured photocurrent as a function of illumination power for 850nm (squares) and 940nm (diamonds) light with grounded back gate (V_{BG} = 0). Lines are a guide to the eye. (e) V_{BG}-dependent photo-responsivity to 850nm light (excitation frequency 225 Hz, illumination power 1.5 mW/cm^2). (f) Dependence of maximum photo-responsivity (V_{BG} = -10 V, illumination power 1.2-1.5 mW/cm^2) on wavelength of exciting light, and corresponding photoconductive gain (assuming a quantum efficiency of 1, see ref. 23). The excitation frequency in panels (d)-(f) is 225 Hz, and all measurements were taken at ~120 K.

Figure 6: Schematic band structure diagram of FGO-MoS_2 heterostructure devices with back gate bias V_{BG} at the threshold voltage V_{th} (a), below it (b) and above it (c).

Figure 1.

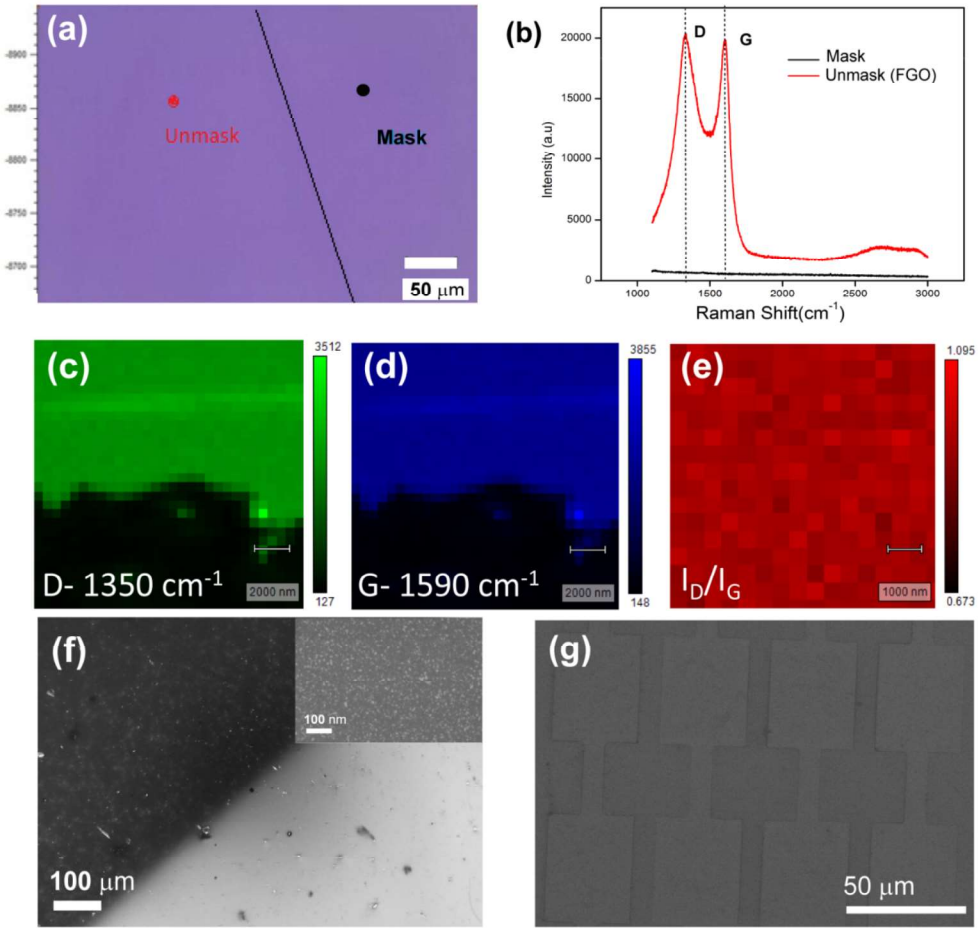
(a)
Unmask
Mask
50 μm
(b)
D
G
Mask
Unmask (FGO)
Intensity (a.u)
Raman Shift(cm-1)
(c)
D- 1350 cm-1
2000 nm
3512
127
(d)
G- 1590 cm-1
2000 nm
3855
148
(e)
ID/IG
1000 nm
1.095
0.673
(f)
100 nm
100 μm
(g)
50 μm

Figure 2.

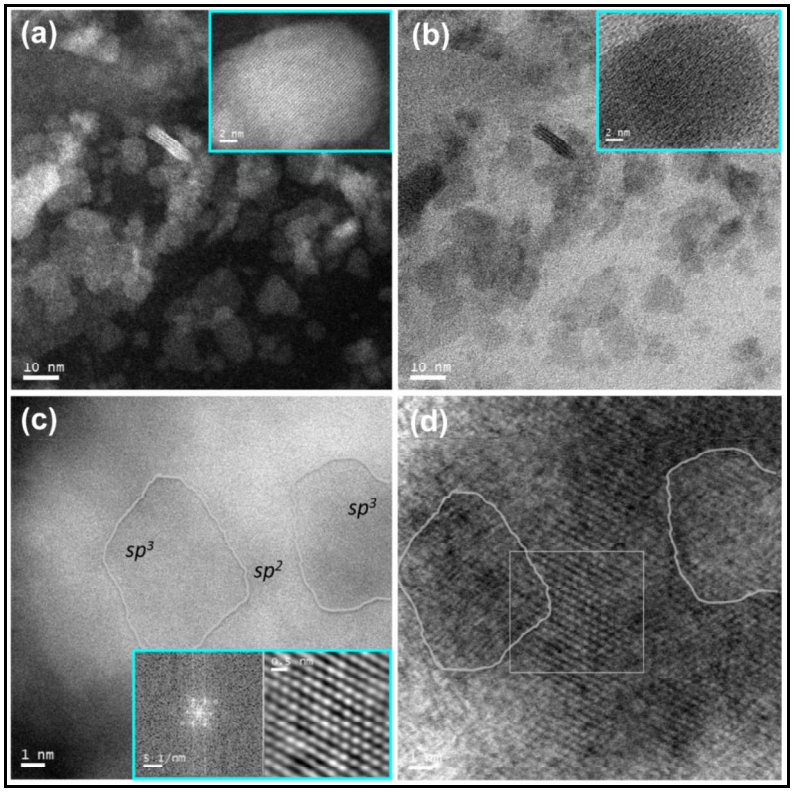

Figure 3.

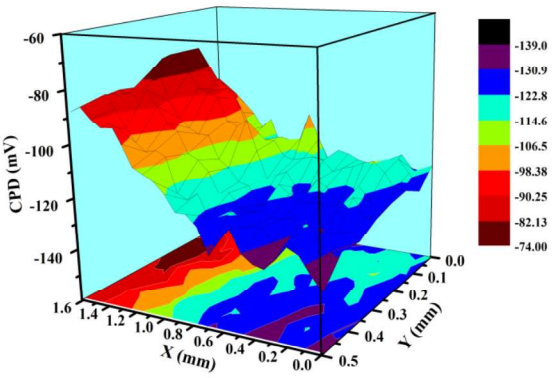
-60
-80
-100
-120
-140
CPD (mV)
1.6
1.4
1.2
1.0
0.8
0.6
0.4
0.2
0.0
X (mm)
0.0
0.1
0.2
0.3
0.4
0.5
Y (mm)
-139.0
-130.9
-122.8
-114.6
-106.5
-98.38
-90.25
-82.13
-74.00

Figure 4.

(a)

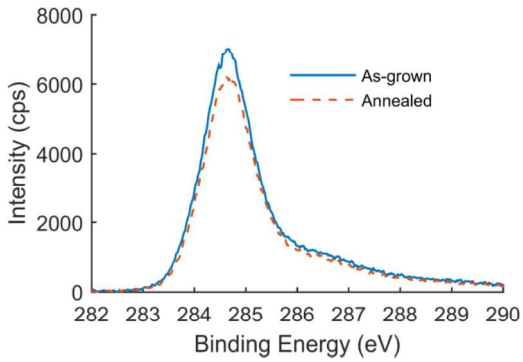
8000
6000
4000
2000
0
Intensity (cps)
282 283 284 285 286 287 288 289 290
Binding Energy (eV)
As-grown
Annealed

(b)

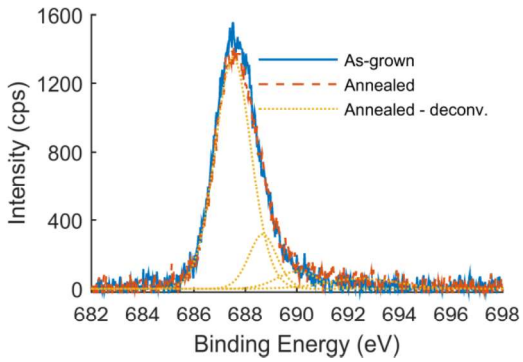
1600
1200
800
400
0
Intensity (cps)
682 684 686 688 690 692 694 696 698
Binding Energy (eV)
As-grown
Annealed
Annealed - deconv.

Figure 5.

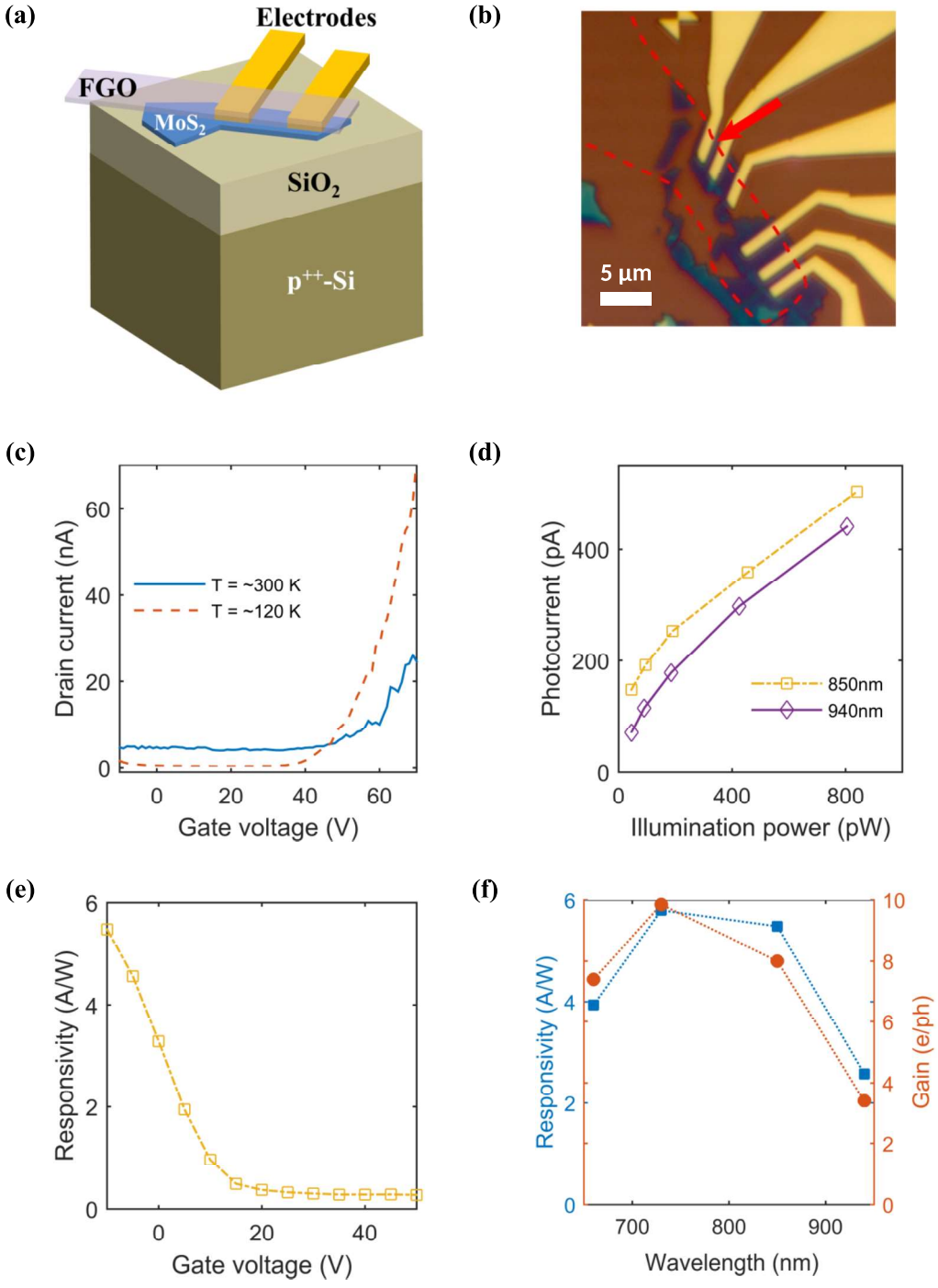
(a)
Electrodes
FGO
MoS2
SiO2
p++-Si
(b)
5 μm
(c)
Drain current (nA)
T = ~300 K
T = ~120 K
Gate voltage (V)
(d)
Photocurrent (pA)
850nm
940nm
Illumination power (pW)
(e)
Responsivity (A/W)
Gate voltage (V)
(f)
Responsivity (A/W)
Gain (e/ph)
Wavelength (nm)

Figure 6.

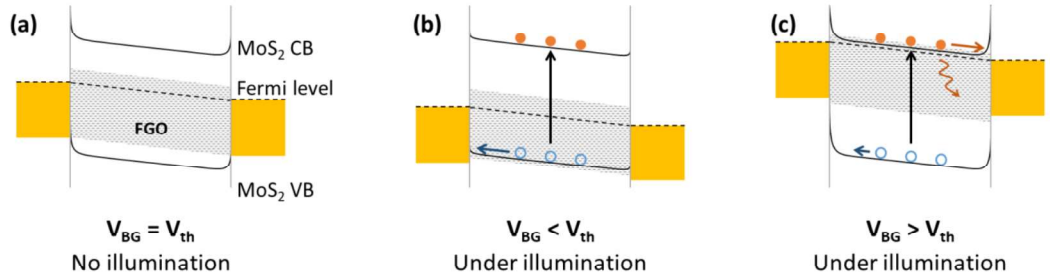
(a)
MoS2 CB
Fermi level
FGO
MoS2 VB
VBG = Vth
No illumination
(b)
VBG < Vth
Under illumination
(c)
VBG > Vth
Under illumination